

PIV investigation on the flow characteristics of a master-slave fluidic oscillator

Ziyan Li¹, Jiajun Liu¹, Di Peng¹, Wenwu Zhou¹, Yingzheng Liu¹, Xin Wen^{1*}

¹Shanghai Jiao Tong University, Institute of Turbomachinery, Shanghai, China

*wenxin84@sjtu.edu.cn

Abstract

The fluidic oscillator can generate continuous sweeping jets based solely on its internal geometry without any moving parts. Therefore, the fluidic oscillator has aroused wide interest in flow control due to its large frequency bandwidth, unsteady control, large coverage area, and robustness. However, applications of the traditional design also have some limitations. The sweeping frequency cannot be controlled independently, but is almost linearly coupled with the jet volume flow rate. In addition, it is very challenging to synchronize the sweeping motions of multiple jets, in order to avoid possible collisions. In this regard, a new design of the master-slave fluidic oscillator is developed. The master and slave layer are fed independently. Not like the continuous jet actuator, the master oscillator can generate pulsed flow through the two discrete exits. The pulsed flow then exerts periodic side force on the steady flow in the slave jet through the control inlets. Current design is proved to produce a continuous sweeping jet with the oscillation frequency decoupled from volume flow rate. Preliminary results from our experiments in a water tank confirmed the control authority. What's more, by fixing the total flow rate, the spreading angle of the ejected jet can be increased with the volume flow rate ratio, and the jet can smoothly change its shape from a steady impinging jet to a sweeping impinging jet with a large spreading angle exceeding 100°.

1 Introduction

Fluidic oscillator, due to its excellent scalability and integration, high frequency bandwidth, robustness, and oscillatory nature, is attracting intensive interest in the field of flow control (Woszidlo, 2011). Though, a marked intrinsic property of the actuator limits its wider applications, that is the linearity of oscillation frequency with volume flow rate. According to Greenblatt and Wygnanski's statistics (Greenblatt and Wygnanski, 2000) on the control of flow separation by periodic excitation, the reduced actuation frequency is usually effective in the range of 0.3~4. Therefore, the decoupling of oscillation frequency and flow rate is significantly essential to the promotion of fluidic oscillators in the flow control field.

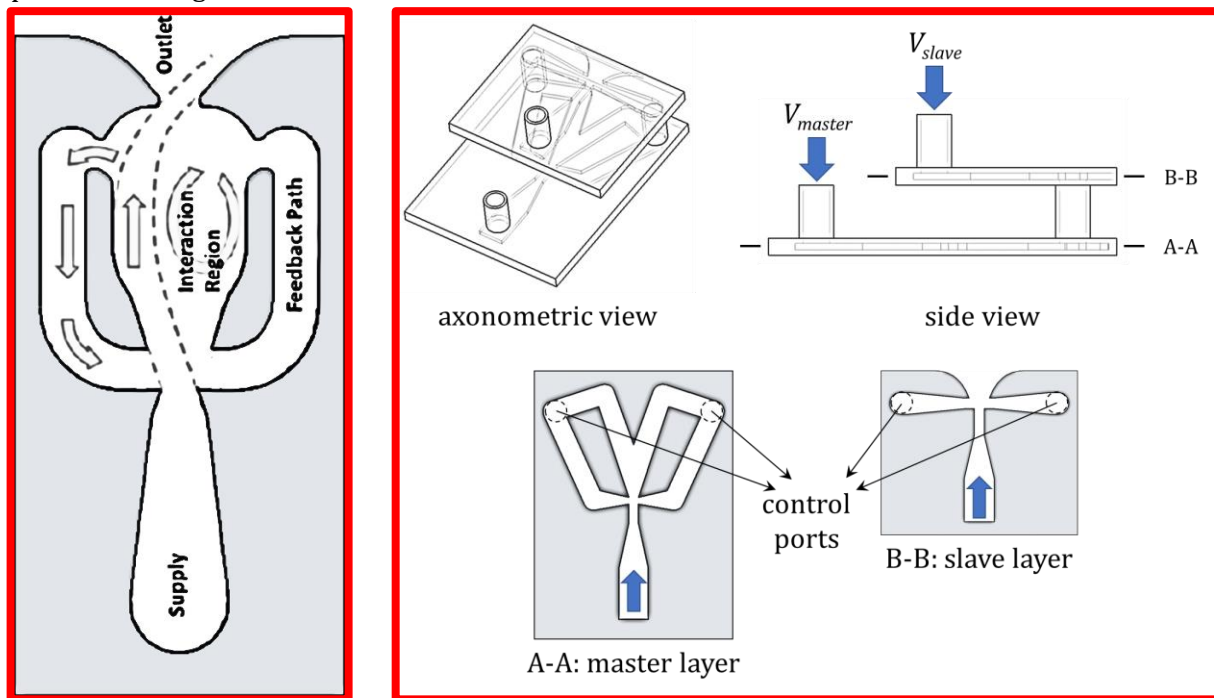
Considerable attempts have been made to decouple this dependence. There mainly involves two approaches. One is still solely based on fluid logic (thus can be reckoned as a "pure" fluidic oscillator) (Bettrich and Niehuis, 2016; Koklu, 2016; Tomac and Sundström, 2019). Koklu (2016) designed a layered fluidic oscillator having decoupled frequency and amplitude control, which is a typical case in point. Another strategy is with the aid of external forces, thus being more direct and controllable (Gregory et al., 2005; Gregory et al., 2009; Gregory et al., 2007). Gregory et al. (2005; 2009; 2007)

designed a variable-frequency fluidic oscillator driven by piezoelectric devices. Since this method relies on the external electric excitation (but still includes a certain fluidic mechanism, i.e. the Coanda effect, when the jet deflects it tends to stick to the solid surface), this type of design can be more regarded as an "impure" fluidic oscillator. These two methods have their own merits. The former inherits the original simplicity and integrity, and thus can be more robust and reliable in severe environments, while the latter shows a more effective modulate property in a wider range of frequency regardless of flowrate ratio, compressibility and other factors.

This paper focuses on the first design concept, which is herein referred to as the "master-slave fluidic oscillator". Time-resolved particle image velocimetry (TR-PIV) is employed to investigate the detailed oscillation characteristic of the master-slave fluidic oscillator. By extracting the velocity and turbulence information of the emitted external jet, a basic understanding can be gained on the actuator's promising applications in the flow control field.

2 Experimental methods

Traditional fluidic oscillator is displayed in Fig. 1(a), while the internal geometry of the master-slave fluidic oscillator is shown in Fig. 1(b). The structure of this novel design has two layers: one is the master layer, which essentially resembles the traditional oscillator in Fig. 1(a), except the discrete-exit design so as to guide the outflow into two exit channels; another is the slave layer, which is composed of a main channel where a steady jet is emitted, and two feedback channels which are separately connected to the aforementioned control ports in the master layer. It's clear that the feedback holes locating on the two sides of the main flow channel provide the motivation of oscillation and turn a steady jet to an oscillating one. The exit throat is a square of 10 mm × 2.5 mm with its aspect ratio being 4.



(a) traditional fluidic oscillator

(b) master-slave fluidic oscillator

Figure 1: Internal structures of 2 types of fluidic oscillators.

As shown in Fig. 2, the experiments were conducted in a water tank which has enough space to avoid sidewall effect on the free jet. The master and slave layers were connected to two non-intersecting flow passages supplied by a pump. Two identical flow meters with an uncertainty level of 2.5% were used to measure the volume flow rates of the master and slave inlet separately. By controlling the flow rate, the corresponding Reynolds number Re , based on the hydraulic diameter of the slave oscillator D_h and jet velocity at the exit throat U_{sj} , ranges from 3893 to 5191. The origin of the coordinate system is set at the middle point of the exit; the x axis points to the streamwise direction and y axis the transverse direction, as shown in Fig. 2.

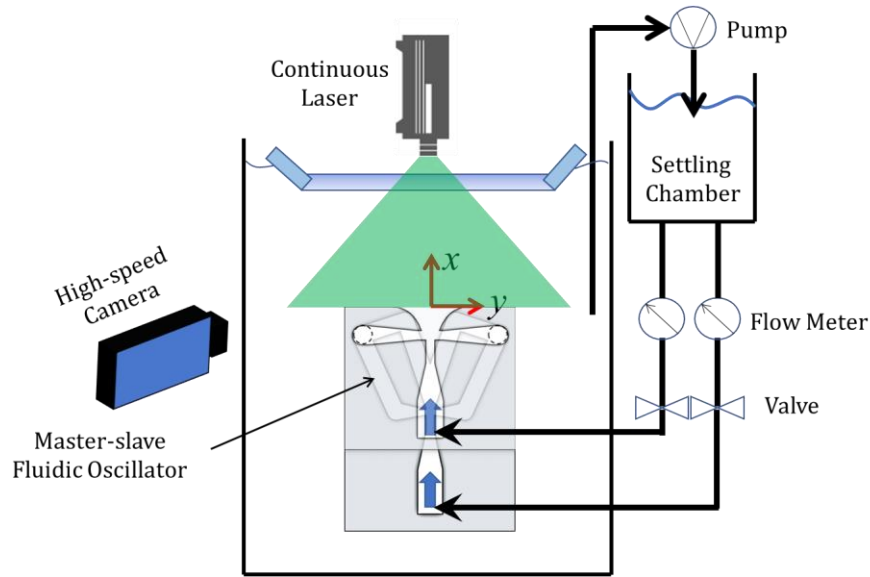


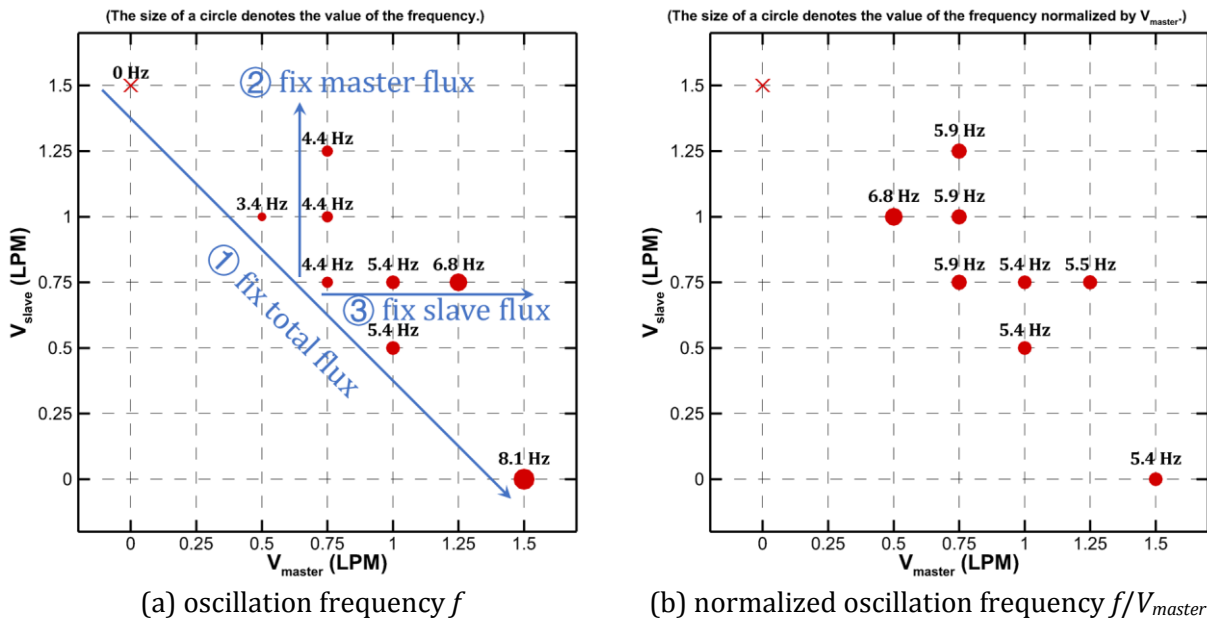
Figure 2: Sketch of experimental setup.

The flow fields were measured by a TR-PIV system. Glass beads with a density $\rho \approx 1050 \text{ kg/m}^3$ and a diameter $d \approx 20 \text{ }\mu\text{m}$ were seeded throughout the water tank as tracer particles. A 5-watt continuous laser (MGL-N-532a-5w, CNI) was used to generate a 2-dimensional laser sheet with a narrow thickness of around 1 mm to illuminate the tracking particles. A high-speed camera (dimax HS4, pco.) was used to capture the illuminated region. The frame rate fixed at 4000 Hz can well resolve the particle movement at jet Reynolds numbers ranging from 3893 to 5191. The exposure time was 50 μs to guarantee sufficiently bright snapshots and meanwhile avoid the trailing of particles. A PIV software package, Micro-Vec (PIVTec, China), was used to calculate vector maps from the particle images. A multigrid cross-correlation technique, in combination with subpixel recognition by Gaussian fitting, was applied. The interrogation window for calculating the correlation was 32×32 pixels with a 50% overlap. As a result, a spatial resolution of about 2 mm was obtained in the velocity vector field of free jet.

3 Results

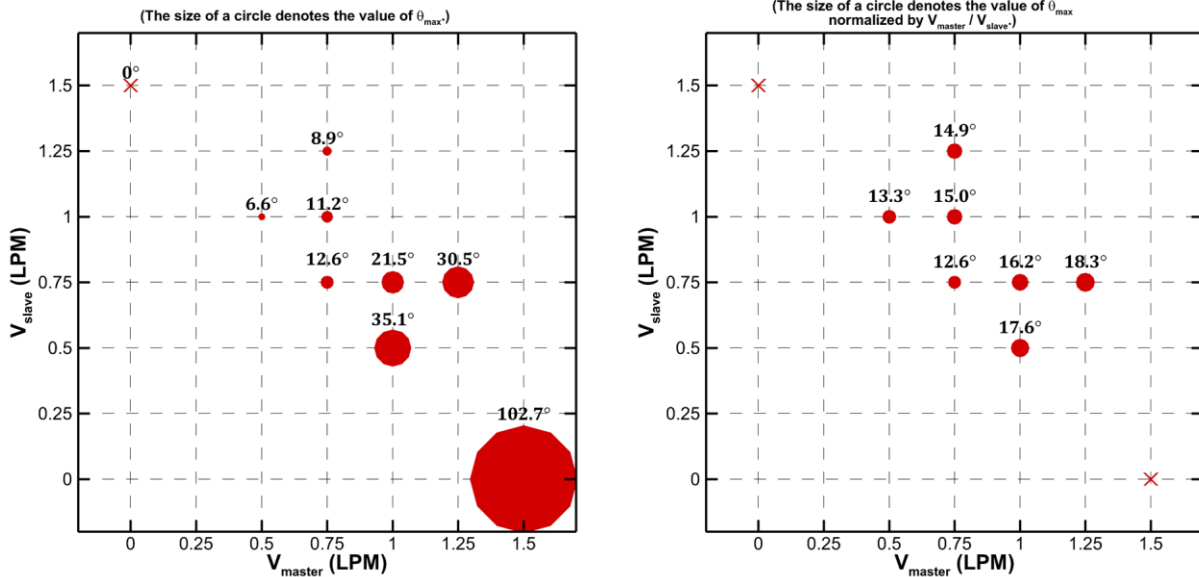
To give a general overview of the oscillation property of the master-slave fluidic oscillator, the oscillation frequency f and the spreading angle θ_{max} under all experimental conditions are displayed in Figs. 3 and 4. In Fig. 3, along the line marked by "①" are five experimental conditions of unity volume flow rate ratio VR . Here, the flow rate ratio VR is defined as the ratio of the volume flow rate at the master inlet V_{master} to that at the slave inlet V_{slave} . It's obvious that the oscillation frequency f increases with the flow rate ratio VR . To find out the dominant variable changing oscillation frequency

f , between the two volume flow rates, one is changed while keeping another constant. The line marked by "②" denotes that V_{master} is fixed while V_{slave} changes, and reverse is the line marked by "③". It's obvious that the oscillation frequency f cannot be changed by slave flux V_{slave} but increases with master flux V_{master} . It's not surprising, because as introduced precedingly about the structure of the layered fluidic oscillator, it's the master layer that drives the flux oscillation of control ports located on both sides of the slave jet. Fig. 3 (b) displays the normalized oscillation frequency f/V_{master} . For a traditional fluidic oscillator (as indicated in Fig. 1), this value is constant as long as the size and the internal structure is hold (Bobusch et al., 2013; Gaertlein et al., 2014; Schmidt et al., 2017; Wen et al., 2018; Woszidlo et al., 2015). This trend exactly reappears in large master flow rates V_{master} for the master-slave fluidic oscillator, but distorts more as V_{master} is closer to zero.



(a) oscillation frequency f (b) normalized oscillation frequency f/V_{master}
 Figure 3: Oscillation frequency under all experimental conditions.

Fig. 4 displays the spreading angle θ_{max} of the master-slave fluidic oscillator under all experimental conditions. Since the master flux promotes oscillation while the slave counterpart restrains oscillation (hold the shape of a steady jet), it can be convincingly deduced that the spreading angle θ_{max} increases with the master flow rate V_{master} but decreases with the slave counterpart V_{slave} . However, it can be a little bit beyond expectation that values of the normalized spreading angle θ_{max}/VR are very close provided that neither the master flow rate V_{master} nor the slave counterpart V_{slave} is too small, as shown by Fig. 4 (b), while there exhibits no simple linear relationship between the spreading angle θ_{max} and the flow rate V for a traditional fluidic oscillators (Gaertlein et al., 2014; Wen and Liu, 2018; Wen et al., 2018; Woszidlo et al., 2015). This finding may make it possible to approximately predict the impact region of the master-slave fluidic oscillator regardless of the volume flow rate ratio VR .



(a) spreading angle θ_{max} (b) normalized spreading angle θ_{max}/VR
 Figure 4: Spreading angle under all experimental conditions.

After a basic investigation of jet property, Figs. 5 ~ 7 explicitly show the influence of the master flow rate V_{master} , the slave flow rate V_{slave} , and the volume flow rate ratio VR on the velocity and turbulence fields. From Fig. 5, as the total flow rate (the summation of V_{master} and V_{slave}) is kept constant, the more the volume flow rate ratio VR , the wider but shorter the impact region. In addition, due to the larger impact region at larger VR , the time-averaged peak velocity inevitably declines, but the peak turbulence intensity Tu is nearly constant. This difference lies in the truth that the intensified sweeping motion as VR is large can to a large extent result in a stronger turbulence fluctuation, but for a single point, the time-averaged velocity decreases.

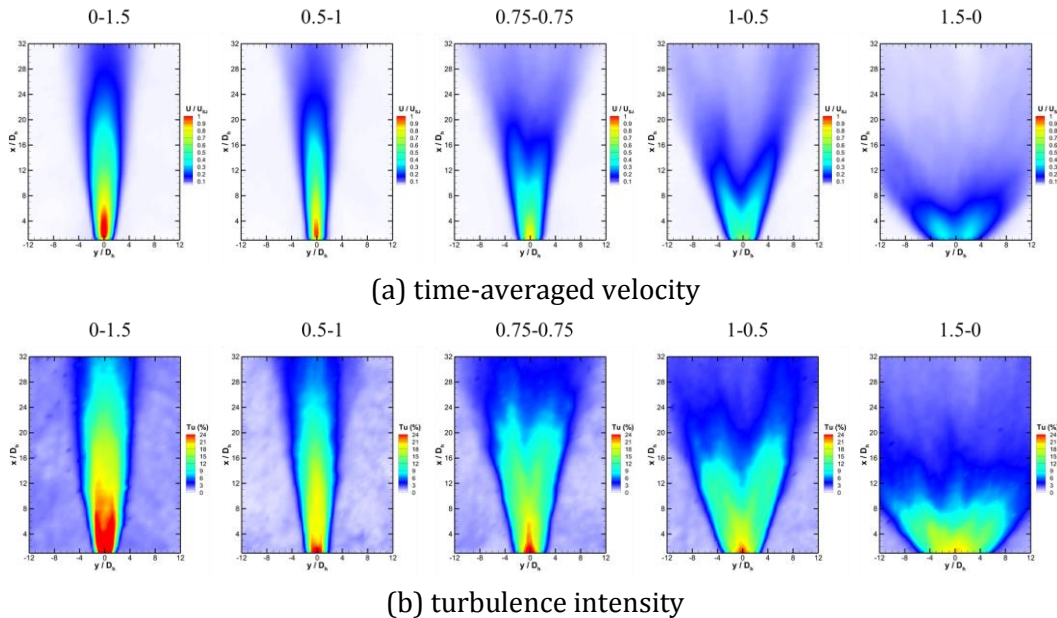
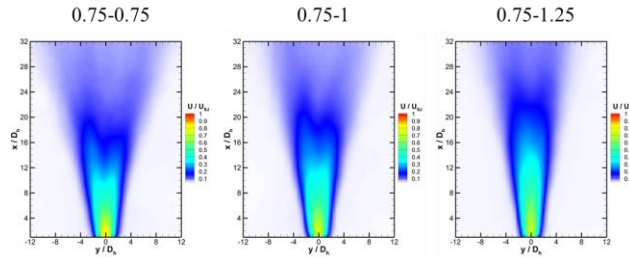
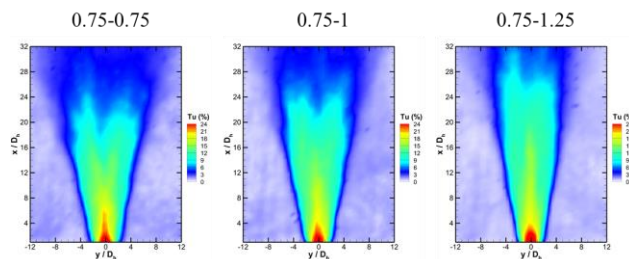


Figure 5: Comparison of time-averaged velocity and turbulence intensity fields when the total flow rate (the summation of V_{master} and V_{slave}) is constant (the two numbers above each figure denote " V_{master} - V_{slave} ", and the unit is LPM; the volume flow rate VR increases from left to right).

Fig. 6 compares the time-averaged velocity and turbulence intensity fields when the master flow rate V_{master} is fixed. Fig. 7 replaces the independent variable and the slave flow rate V_{slave} is fixed. As intuitively shown, the increase in the master flow contributes to the spreading of ejected flow, which is much favorable for the mixing goal and hence flow control applications; contrast to this, the increase in the slave flow helps to hold the rigidity of the jet, making the flow penetrate to further regions. The turbulence fields are strongly correlated with the velocity fields and therefore exhibit similar features.

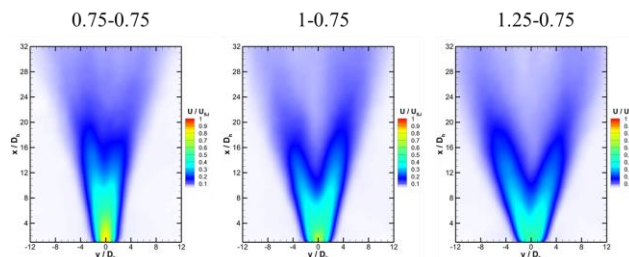


(a) time-averaged velocity

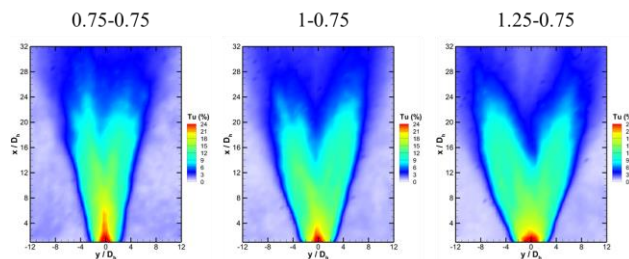


(b) turbulence intensity

Figure 6: Comparison of time-averaged velocity and turbulence intensity fields when the master flow rate V_{master} is constant (the two numbers above each figure denote " $V_{master}-V_{slave}$ ", and the unit is LPM; the slave flow rate V_{slave} increases from left to right).



(a) time-averaged velocity



(b) turbulence intensity

Figure 7: Comparison of time-averaged velocity and turbulence intensity fields when the slave flow rate V_{slave} is constant (the two numbers above each figure denote " $V_{master}-V_{slave}$ ", and the unit is LPM; the master flow rate V_{master} increases from left to right).

From the above-introduced characteristics, it can be very easy to see the promising merits of the master-slave fluidic oscillator. First, it overcomes the linear dependence of oscillation frequency on volume flow rate, thus broadening the available frequency band in flow control applications. Second, only by adjusting the share of volume flow rate between the master and slave inlets, the ejected jet can smoothly change its shape from a steady impinging jet to a sweeping impinging jet with a large spreading angle exceeding 100° , which means the impact region can be regulated arbitrarily or based on actual situations. Third, the oscillation pattern nearly approaches a sinusoidal wave (not displayed due to the reason of paper length) under all tested experimental conditions, which is expected to generate an even jet momentum distribution in space compared to traditional fluidic oscillators.

4 Conclusion

A novel fluidic oscillator which can produce a continuous sweeping jet with the oscillation frequency decoupled from volume flow rate is investigated by 2-dimensional TR-PIV in a water tank. This is achieved by employing the double-layer structure and connecting the discrete exits in the master layer to the control ports in the slave layer. Preliminary results from our experiments in a water tank confirmed the control authority. What's more, by fixing the total flow rate, the time-averaged flow fields obtained from PIV measurement revealed that the spreading angle of the ejected jet can be increased by increasing the volume flow rate ratio, and the jet can smoothly change its shape from a steady impinging jet to a sweeping impinging jet with a large spreading angle exceeding 100° . Above characteristics can strongly prove the bright prospect of the master-slave fluidic oscillator in flow control fields. Further works will be done to reveal the internal flow interaction and optimize the design to achieve a more effective control on both single and multiple slave jets.

Acknowledgements

The authors gratefully acknowledge the financial support from the National Natural Science Foundation of China (Grant nos. 11702172 and 11725209) extended to this study.

References

- Bettrich V, and Niehuis R (2016) Experimental Investigations of a High Frequency Master-Slave Fluidic Oscillator to Achieve Independent Frequency and Mass Flow Characteristics. In *ASME 2016 International Mechanical Engineering Congress and Exposition, Phoenix, Arizona, USA, November 11-17*
- Bobusch BC, Woszidlo R, Bergada JM, Nayeri CN, and Paschereit CO (2013) Experimental study of the internal flow structures inside a fluidic oscillator. *Experiments in Fluids* 54:1559
- Gaertlein S, Woszidlo R, Ostermann F, Nayeri C, and Paschereit CO (2014) The time-resolved internal and external flow field properties of a fluidic oscillator. In *52nd Aerospace Sciences Meeting, National Harbor, Maryland, USA, January 13-17*
- Greenblatt D, and Wygnanski IJ (2000) The control of flow separation by periodic excitation. *Progress in Aerospace Sciences* 36:487-545

- Gregory JW, Gnanamanickam E, Sullivan J, and Raghu S (2005) Variable-Frequency Fluidic Oscillator Driven by Piezoelectric Devices. In *43rd AIAA Aerospace Sciences Meeting and Exhibit, Reno, Nevada, USA, January 10 - 13*
- Gregory JW, Gnanamanickam EP, Sullivan JP, and Raghu S (2009) Variable-Frequency Fluidic Oscillator Driven by a Piezoelectric Bender. *AIAA Journal* 47:2717-2725
- Gregory JW, Ruotolo JC, Byerley AR, and McLaughlin TE (2007) Switching behavior of a plasma-fluidic actuator. In *45th AIAA Aerospace Sciences Meeting and Exhibit, Reno, Nevada, USA, January 8 - 11*
- Koklu M (2016) U.S. Patent No. US 9,339,825 B2.
- Schmidt HJ, Woszidlo R, Nayeri CN, and Paschereit CO (2017) Separation control with fluidic oscillators in water. *Experiments in Fluids* 58:106
- Tomac MN, and Sundström E (2019) Adjustable Frequency Fluidic Oscillator with Supermode Frequency. *AIAA Journal* 0:1-11
- Wen X, and Liu Y (2018) Lagrangian analysis of sweeping jets measured by time-resolved particle image velocimetry. *Experimental Thermal and Fluid Science* 97:192-204
- Wen X, Liu Y, and Tang H (2018) Unsteady behavior of a sweeping impinging jet: Time-resolved particle image velocimetry measurements. *Experimental Thermal and Fluid Science*:96:111-127
- Woszidlo R (2011) PARAMETERS GOVERNING SEPARATION CONTROL WITH SWEEPING JET ACTUATORS. (DOCTOR OF PHILOSOPHY), The University of Arizona. Retrieved from <http://hdl.handle.net/10150/203475>
- Woszidlo R, Ostermann F, Nayeri CN, and Paschereit CO (2015) The time-resolved natural flow field of a fluidic oscillator. *Experiments in Fluids* 56:125